Reconstruction de défauts dans les plaques élastiques à l'aide d'ondes de Lamb localement résonantes

Angèle Niclas

Join work with
Éric Bonnetier, Claire Prada, Laurent Seppecher, Grégory Vial

16/06/2022

Context

Goal: Non destructive monitoring of industrial structures like metal plates, boat hulls, aircraft parts, bridges, rain tracks...

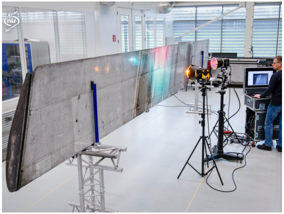

Figure: Industrial monitoring of a large aircraft part.

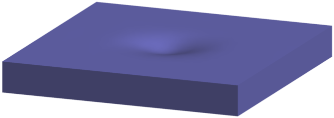

Figure: Width defect in a 3D elastic plate.

Context

Goal: Non destructive monitoring of industrial structures like metal plates, boat hulls, aircraft parts, bridges, rain tracks...

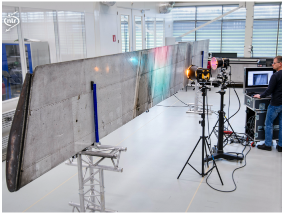

Figure: Industrial monitoring of a large aircraft part.

Figure: Width defect in a 2D elastic plate.

Modal decomposition

A source $\boldsymbol{f}$ generates an elastic displacement field $\boldsymbol{u}$ satisfying

$$\begin{cases} \nabla \cdot \boldsymbol{\sigma}(\boldsymbol{u}) + \omega^2 \boldsymbol{u} = \boldsymbol{f} & \text{in } \Omega, \\ \boldsymbol{\sigma}(\boldsymbol{u}) \cdot \nu = 0 & \text{on } \partial\Omega, \end{cases} \tag{1}$$

where Ω is the plate, $\boldsymbol{\sigma}$ the stress tensor, ω the frequency.
Modal decomposition at width h for almost every $\omega \in \mathbb{R}_+$:

$$\boldsymbol{u}(x, y) = \sum_{n>0} (a_n(x) u_n(y), b_n(x) v_n(y)), \tag{2}$$

Modal decomposition

A source $\boldsymbol{f}$ generates an elastic displacement field $\boldsymbol{u}$ satisfying

$$\begin{cases} \nabla \cdot \boldsymbol{\sigma}(\boldsymbol{u}) + \omega^2 \boldsymbol{u} = \boldsymbol{f} & \text{in } \Omega, \\ \boldsymbol{\sigma}(\boldsymbol{u}) \cdot \nu = 0 & \text{on } \partial\Omega, \end{cases} \tag{1}$$

where Ω is the plate, $\boldsymbol{\sigma}$ the stress tensor, ω the frequency.
Modal decomposition at width h for almost every $\omega \in \mathbb{R}_+$:

$$\boldsymbol{u}(x,y) = \sum_{n>0} (a_n(x) u_n(y), b_n(x) v_n(y)), \tag{2}$$

(u_n, v_n) are Lamb modes associated to the wavenumber $k_n \in \mathbb{C}$.

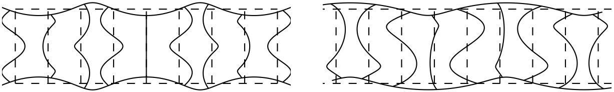

Figure: Elastic deformation of a plate $e^{ik_n x}(u_n(y), v_n(y))$ for a symmetric and an anti-symmetric Lamb mode.

State of the art

Usual experimental setup:

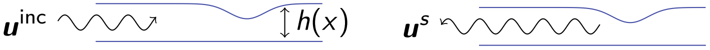

[1] Bourgeois, Lunéville. The linear sampling method in a waveguide: A modal formulation. Inverse Problems, 2008.
[2] Ammari, Iakovleva, Kang. Reconstruction of a small inclusion in a two- dimensional open waveguide. SIAM Journal on Applied Mathematics, 2005.
[3] Bonnetier, Niclas, Seppecher, Vial. Small defects reconstruction in waveguide from multifrequency one-side scattering data. Inverse Problems & Imaging, 2022.

State of the art

Usual experimental setup:

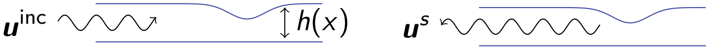

- One frequency ω, different incident waves: Linear sampling method, Far-field asymptotic developments...
- Different frequencies ω, one incident wave: MUSIC algorithm, Born approximations...

[1] Bourgeois, Lunéville. The linear sampling method in a waveguide: A modal formulation. Inverse Problems, 2008.
[2] Ammari, Iakovleva, Kang. Reconstruction of a small inclusion in a two- dimensional open waveguide. SIAM Journal on Applied Mathematics, 2005.
[3] Bonnetier, Niclas, Seppecher, Vial. Small defects reconstruction in waveguide from multifrequency one-side scattering data. Inverse Problems & Imaging, 2022.

State of the art

Usual experimental setup:

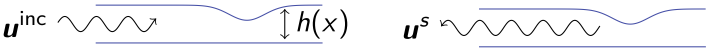

- One frequency ω, different incident waves: Linear sampling method, Far-field asymptotic developments...
- Different frequencies ω, one incident wave: MUSIC algorithm, Born approximations...

$\Rightarrow$ Avoid the so-called resonant frequencies.

[1] Bourgeois, Lunéville. The linear sampling method in a waveguide: A modal formulation. Inverse Problems, 2008.
[2] Ammari, Iakovleva, Kang. Reconstruction of a small inclusion in a two- dimensional open waveguide. SIAM Journal on Applied Mathematics, 2005.
[3] Bonnetier, Niclas, Seppecher, Vial. Small defects reconstruction in waveguide from multifrequency one-side scattering data. Inverse Problems & Imaging, 2022.

Resonant frequencies

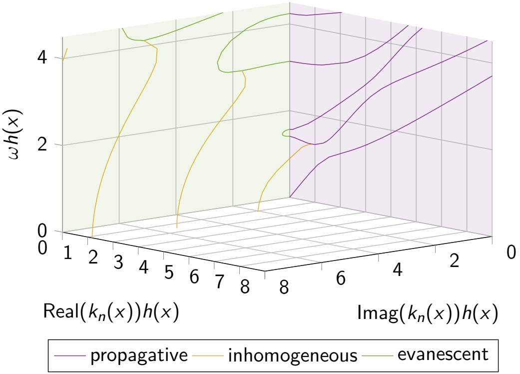

Figure: Rayleigh-Lamb dispersion curves and resonant frequencies. At resonant frequencies, Lamb modal decomposition fails and the elastic problem is not well-posed.

Resonant frequencies

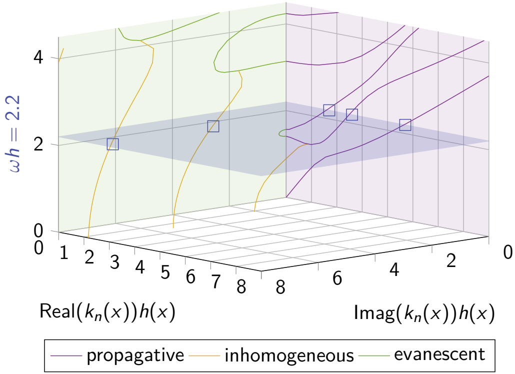

Figure: Rayleigh-Lamb dispersion curves and resonant frequencies. At resonant frequencies, Lamb modal decomposition fails and the elastic problem is not well-posed.

Resonant frequencies

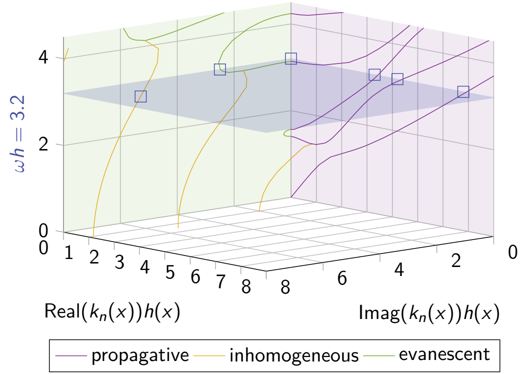

Figure: Rayleigh-Lamb dispersion curves and resonant frequencies. At resonant frequencies, Lamb modal decomposition fails and the elastic problem is not well-posed.

Resonant frequencies

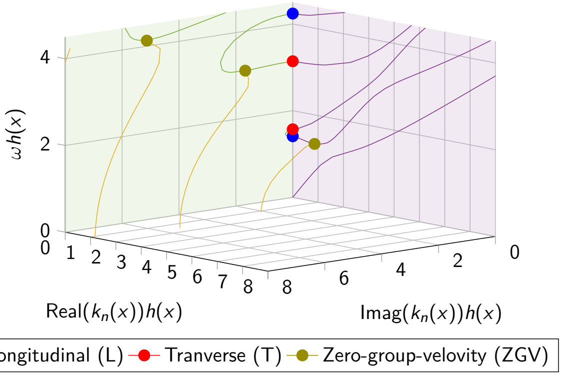

Figure: Rayleigh-Lamb dispersion curves and resonant frequencies. At resonant frequencies, Lamb modal decomposition fails and the elastic problem is not well-posed.

Resonant frequencies

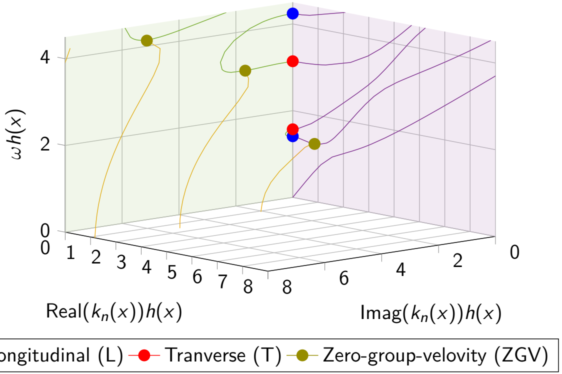

Figure: Rayleigh-Lamb dispersion curves and resonant frequencies. Three types of resonant points. L: $k_n = 0$ and $u_n = 0$. T: $k_n = 0$ and $v_n = 0$. ZGV: $k_n \neq 0$, $u_n, v_n \neq 0$

Experimental setup at Institut Langevin

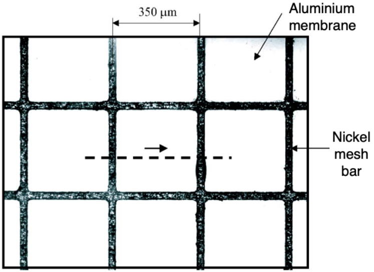

Figure: Response amplitude of a plate with two different widths (white/black) at the resonant frequency of the white area. Measurements are made along the dotted line.

[4] Balogun, Murray, Prada. Simulation and measurement of the optical excitation of the s1 zero group velocity lamb wave resonance in plates. Journal of Applied Physics, 2007.

Experimental setup at Institut Langevin

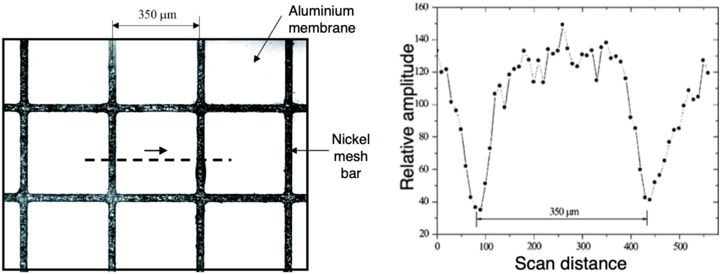

Figure: Response amplitude of a plate with two different widths (white/black) at the resonant frequency of the white area. Measurements are made along the dotted line.

[4] Balogun, Murray, Prada. Simulation and measurement of the optical excitation of the s1 zero group velocity lamb wave resonance in plates. Journal of Applied Physics, 2007.

General setting

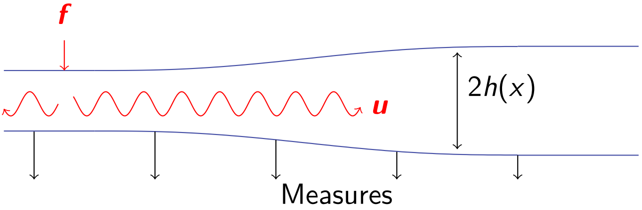

Figure: Slowly varying waveguide of width $2h(x)$.

General setting

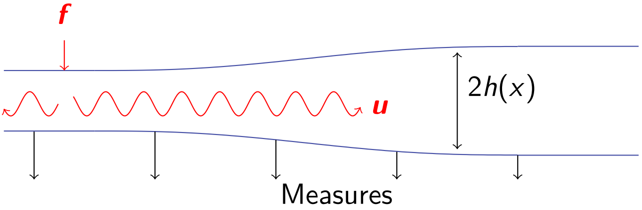

Figure: Slowly varying waveguide of width $2h(x)$.

Modal decomposition:

$$\boldsymbol{u}(x,y) = \sum_{n>0} (a_n(x) u_n(x,y), b_n(x) v_n(x,y)). \tag{3}$$

Issue: if there exists $x^\star$ (called locally resonant point) such that $\omega h(x^\star)$ is resonant then this decomposition fails.

Longitudinal mode

We define the quantity $J_n = \int_{-h(x)}^{h(x)} \boldsymbol{\sigma}(\boldsymbol{u}_n)_2 v_n - \boldsymbol{\sigma}(\boldsymbol{u}_n)_1 u_n$

To avoid the issue at $x^\star$, we introduce a modified Lamb basis

$$\widetilde{u_n} = \frac{u_n}{J_n}, \qquad \widetilde{v_n} = v_n. \tag{4}$$

[5] Pagneux, Maurel. Lamb wave propagation in elastic waveguides with variable thickness. Proceedings of the Royal Society A, 2006.

Longitudinal mode

We define the quantity $J_n = \int_{-h(x)}^{h(x)} \boldsymbol{\sigma}(\boldsymbol{u}_n)_2 v_n - \boldsymbol{\sigma}(\boldsymbol{u}_n)_1 u_n$

To avoid the issue at $x^\star$, we introduce a modified Lamb basis

$$\widetilde{u_n} = \frac{u_n}{J_n}, \qquad \widetilde{v_n} = v_n. \tag{4}$$

This modified basis is complete even at $x^\star$ and we have

$$\begin{cases} b_n'' + k_n(x)^2 b_n = F_1^n, \\ a_n = \dfrac{b_n'}{ik_n(x)} + F_2^n. \end{cases} \tag{5}$$

$\Rightarrow$ We recognize a Schrödinger equation on b_n.

[5] Pagneux, Maurel. Lamb wave propagation in elastic waveguides with variable thickness. Proceedings of the Royal Society A, 2006.

Green function

Using the previous study of the Schrödinger equation, we can approximate b_n and then a_n with the approximated Green function G_n^{app}. For n a locally resonant mode and $s > x > x^\star$,

$$G_n^{\text{app}}(x,s) = C\,\mathcal{A}\left(-\left(\frac{3}{2}\int_{x^\star}^{x} k_n\right)^{2/3}\right). \tag{6}$$

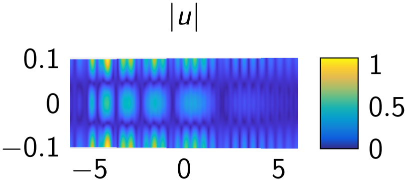

Figure: Wavefield at a longitudinal locally resonant point.

[6] Bonnetier, Niclas, Seppecher, Vial. The Helmholtz problem in slowly varying waveguides at locally resonant frequencies, submitted in Wave Motion, 2022
[7] Niclas, Prada. Reconstruction of shape defects in elastic waveguides using longitudinal, transverse and ZGV resonances, in preparation, 2022

Transverse and zero-group velocity mode

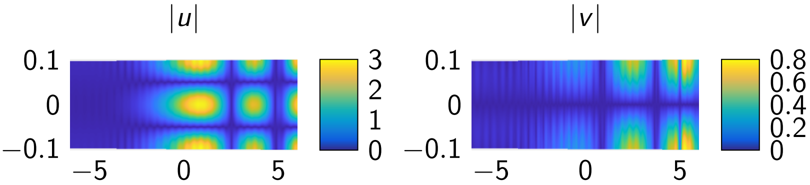

Figure: Wavefield at a transverse locally resonant point.

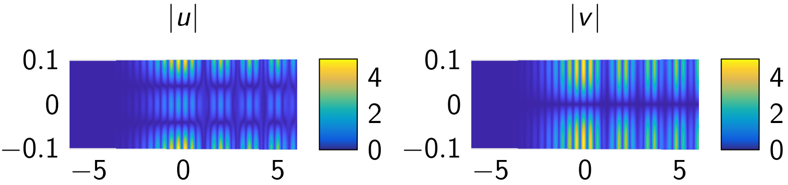

Figure: Wavefield at a zero-group velocity locally resonant point.

Locally resonant point

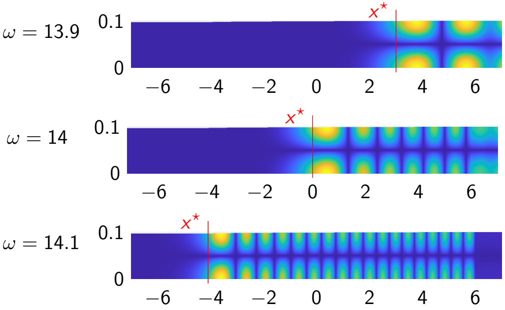

Figure: Wavefield $|u|$ for different transverse locally resonant frequencies.

Locally resonant point

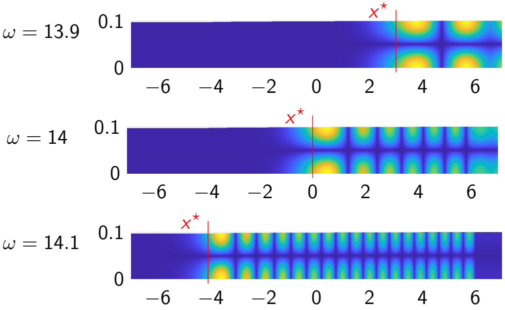

Figure: Wavefield $|u|$ for different transverse locally resonant frequencies.

If we recover the position of $x^\star$, we know the local width

$$h(x^\star) = \omega_{\text{crit}}/\omega. \tag{7}$$

For instance, if $\omega h(x^\star) = 3.2$ then $h(x^\star) = 3.2/\omega$.

Filtering of measurements

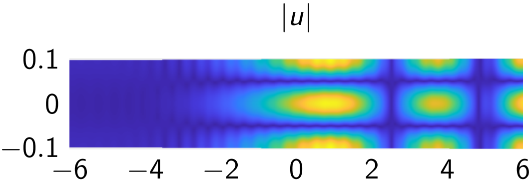

Figure: Measurements and filtering of the data for a transverse locally resonant mode.

Filtering of measurements

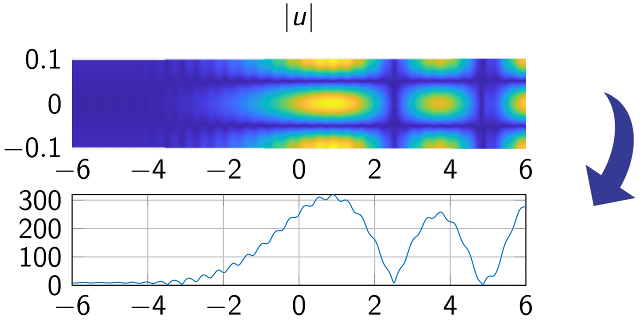

Measurements at the surface

Figure: Measurements and filtering of the data for a transverse locally resonant mode.

Filtering of measurements

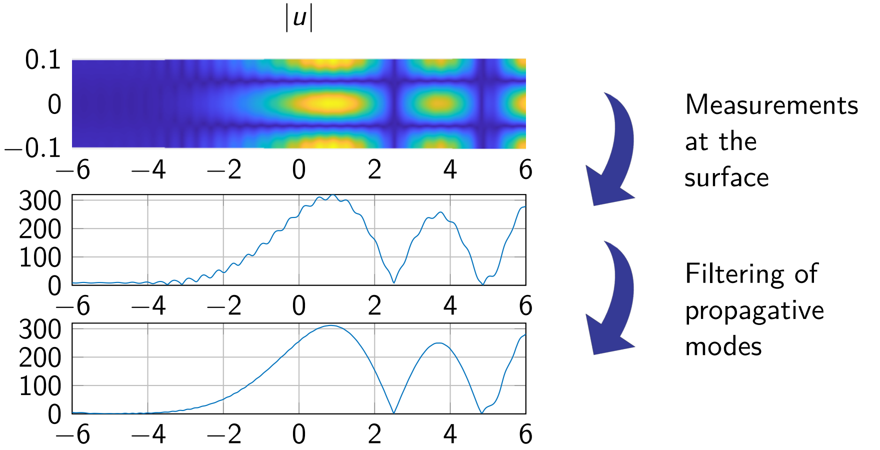

Figure: Measurements and filtering of the data for a transverse locally resonant mode.

Reconstruction of $x^\star$

Doing a Taylor expansion on G_n^{app}, we notice that around $x^\star$, the data d satisfy

$$d \approx z\mathcal{A}(\alpha(x - x^\star)), \tag{8}$$

where $z, \alpha > 0$. We minimize the function

$$J(z, \alpha, x^\star) = \|z\mathcal{A}(\alpha(x - x^\star)) - d\|_2. \tag{9}$$

[8] Niclas, Seppecher. Reconstruction of smooth shape defects in waveguides using locally resonant frequencies surface measurements, submitted in Inverse Problems, 2022

Reconstruction of $x^\star$

Doing a Taylor expansion on G_n^{app}, we notice that around $x^\star$, the data d satisfy

$$d \approx z\mathcal{A}(\alpha(x - x^\star)), \tag{8}$$

where $z, \alpha > 0$. We minimize the function

$$J(z, \alpha, x^\star) = \|z\mathcal{A}(\alpha(x - x^\star)) - d\|_2. \tag{9}$$

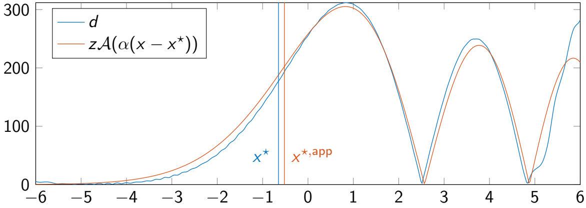

Figure: Comparison between the data d and the Airy function obtained by minimizing J.

[8] Niclas, Seppecher. Reconstruction of smooth shape defects in waveguides using locally resonant frequencies surface measurements, submitted in Inverse Problems, 2022

Reconstruction of h

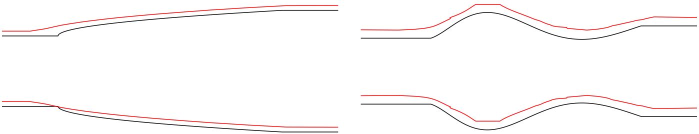

Figure: Reconstruction of two width profiles. Black: initial shape. Red: reconstruction slightly shifted for comparison purposes.

$\|h'\|_\infty$	9.10^{-4}	3.10^{-3}	7.10^{-3}	1.10^{-2}
L, $\|h - h^{\text{app}}\|_\infty / \|h\|_\infty$	2.8%	7.6%	13.2%	23.4%
T, $\|h - h^{\text{app}}\|_\infty / \|h\|_\infty$	2.9%	5.3%	10.2%	17.4%
ZGV, $\|h - h^{\text{app}}\|_\infty / \|h\|_\infty$	1.7%	2.3%	5.7%	8.2%

Table: Relative errors on the reconstruction for increasing values of $\|h'\|_\infty$

Conclusion

Main results:

- A wavefield approximation in slowly varying waveguides near L, T and ZGV resonances
- An efficient and stable multi-frequency method to reconstruct the width with high sensibility

Conclusion

Main results:

- A wavefield approximation in slowly varying waveguides near L, T and ZGV resonances
- An efficient and stable multi-frequency method to reconstruct the width with high sensibility

Outlook:

- Collaboration to test our method on real data
- Generalization when top and bottom of the waveguide vary
- Generalization to quickly variable waveguides

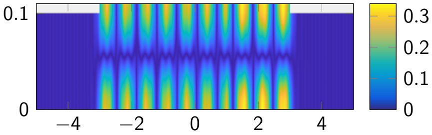

Figure: Numerical simulation of wavefield propagation in a waveguides with width steps.